Polarization switching in a mid-infrared Er:YAlO 3 laser

Florent Cassouret, Ahmed Nady, Pavel Loiko, Simone Normani, Alain Braud, Weidong Chen, Valentin Petrov, Dunlu Sun, Peixiong Zhang, Bruno Viana, et al.

Polarization switching in a mid-infrared Er:$YAlO_3$ laser

Florent Cassouret,[1] Ahmed Nady,[2,3] Pavel Loiko,[2] Simone Normani,[2] Alain Braud,[2] Weidong Chen,[4,5] Valentin Petrov,[5] Dunlu Sun,[6] Peixiong Zhang,[7] Bruno Viana,[8] Ammar Hideur,[9] and Patrice Camy[2,*]

[1]*Division of Research Innovation and Collaboration, Institute for Molecular Science, 38 Nishigonaka, Myodaiji, Okazaki-shi, Aichi-ken, 444-8585, Japan*
[2]*Centre de Recherche sur les Ions, les Matériaux et la Photonique (CIMAP), UMR 6252 CEA-CNRS-ENSICAEN, Université de Caen Normandie, 6 Boulevard Maréchal Juin, 14050 Caen, France*
[3]*Faculty of Science, Beni-Suef University, 62521 Beni Suef, Egypt*
[4]*Fujian Institute of Research on the Structure of Matter, Chinese Academy of Sciences, 350002 Fuzhou, China*
[5]*Max Born Institute for Nonlinear Optics and Short Pulse Spectroscopy, Max-Born-Str. 2a, 12489 Berlin, Germany*
[6]*Anhui Institute of Optics and Fine Mechanics, Hefei Institutes of Physical Science, Chinese Academy of Sciences, 230031 Hefei, China*
[7]*Department of Optoelectronic Engineering, Jinan University, 510632 Guangzhou, China*
[8]*PSL University, Chimie ParisTech – CNRS, Institut de Recherche de Chimie Paris, 11 rue Pierre et Marie Curie, 75005 Paris, France*
[9]*CORIA UMR6614, CNRS-INSA-Université de Rouen Normandie, Normandie Université, 76801 Saint Etienne du Rouvray, France*
*patrice.camy@ensicaen.fr

Received XX Month XXXX; revised XX Month, XXXX; accepted XX Month XXXX; posted XX Month XXXX (Doc. ID XXXXX); published XX Month XXXX

We report on a polarization-resolved study of mid-infrared emission properties of Er^{3+}-doped orthorhombic yttrium aluminum perovskite $YAlO_3$ single crystal. For the $^4I_{11/2}\rightarrow{}^4I_{13/2}$ Er^{3+} transition, the stimulated emission cross-section is 0.20×10^{-20} cm^2 at 2919 nm for light polarization $E \parallel c$. Pumped by an Yb-fiber laser at 976 nm, the 10 at.% Er:$YAlO_3$ laser delivered 1.36 W at 2919 nm with a slope efficiency of 31.4%, very close to the Stokes limit, a laser threshold as low as 33 mW and a linear polarization. Pump-induced polarization switching between $E \parallel b$ and $E \parallel c$ eigen states was observed and explained by excited-state absorption from the terminal laser level. © 2024 Optical Society of America

http://dx.doi.org/10.1364/OL.99.099999

Lasers emitting around 3 μm find applications in medicine (laser surgery), in pumping of mid-infrared coherent sources such as optical parametric oscillators [1], supercontinuum generators [2] and lasers based on Fe^{2+} (e.g. Fe:ZnSe [3]) and Dy^{3+} (e.g. Dy:ZBLAN fiber [4]), and in molecular spectroscopy in the so-called molecular fingerprint region, in particular atmospheric species such as water, carbon monoxide, and methane. Water and hydroxyapatite molecules in biological tissues exhibit strong absorption near 3 μm leading to small penetration depths in bio-tissues and high precision of incisions. For instance, Er:YAG lasers emitting at 2.94 μm are well suited for effective removal of dentin and enamel with only minor side-effects such as thermal damage [5].

Several rare-earth (RE) ions such as Er^{3+}, Ho^{3+} and Dy^{3+} emit around 3 μm [6]. Among them, Er^{3+} is mostly used to generate coherent radiation in this spectral range based on the $^4I_{11/2} \rightarrow {}^4I_{13/2}$ transition [7], Fig. 1(a). Er^{3+}-doped materials can be efficiently pumped at 0.98 μm directly to the upper laser level, e.g., by commercial InGaAs laser diodes. The 3 μm transition of Er^{3+} is self-terminating as the lifetime of the terminal metastable laser level is longer than that of the emitting manifold, $\tau_{lum}(^4I_{13/2}) > \tau_{lum}(^4I_{11/2})$, leading to a bottleneck effect. This can be overcome by using high Er^{3+} doping levels for energy-transfer upconversion (ETU_1) ($^4I_{13/2} + {}^4I_{13/2} \rightarrow {}^4I_{9/2} + {}^4I_{15/2}$) emptying the lower laser level and refilling the emitting state [8]. Furthermore, low phonon energy host matrices are desired to suppress the non-radiative path from the $^4I_{11/2}$ level. Efficient continuous-wave (CW) 3-μm Er solid-state lasers power scalable to the multi-Watt level are known [9,10].

Yttrium aluminum perovskite ($YAlO_3$) is a well-known laser host crystal. It crystallizes in the same binary system (Al_2O_3-Y_2O_3) as yttrium aluminum garnet. The natural birefringence of $YAlO_3$ and the associated polarization anisotropy of emission properties of the dopant RE cations determine linear polarization of laser emission and diminished depolarization losses. $YAlO_3$ also features good thermo-mechanical properties allowing for power scalable operation. Finally, it presents favorable relatively low maximum phonon energy ($h\nu_{ph}$ = 551 cm^{-1}) for an oxide crystal, as evidenced by the polarized Raman spectra shown in Fig. 1(b). This is essential for laser operation at wavelengths above 2 μm [11].

Er^{3+}-doped $YAlO_3$ crystals have been already employed in 3 μm lasers [7,10,12]. A diode-pumped 5 at.% Er:$YAlO_3$ laser delivered 6.9 W at 2920 nm with a slope efficiency of 30.6% [10]. A 2.92 μm Er:$YAlO_3$ laser was used in [3] for efficient pumping of a 4.1 μm

Fe^{2+}:ZnSe laser. However, only unpolarized spectroscopy of Er:$YAlO_3$ can be found in the literature[13-15].

Further progress in the development of efficient 3-μm Er:$YAlO_3$ lasers and amplifiers [10,16] demand accurate knowledge of the polarization anisotropy of its emission properties. In this Letter, we report on polarized stimulated-emission and gain cross-sections of Er^{3+}:$YAlO_3$, and validate the results by explaining the polarization switching effect in a 3-μm Er:$YAlO_3$ laser. We also prove the suitability of commercial 976 nm Yb-fiber lasers (YFLs) for efficient pumping of Er:$YAlO_3$ leading to a low-threshold lasing.

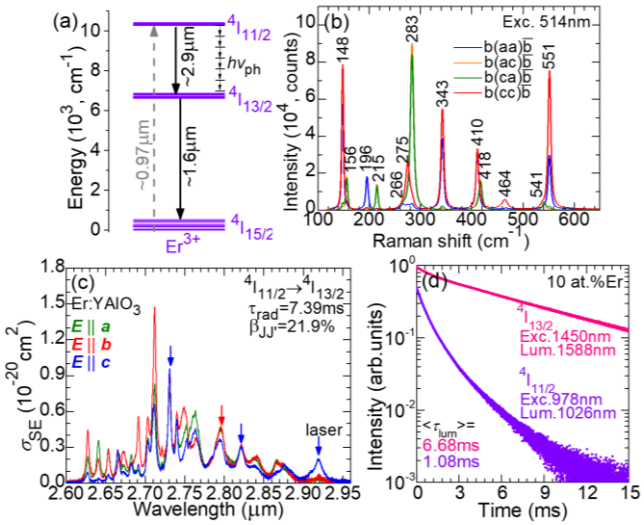

Fig. 1. (a) Partial energy-level scheme of Er^{3+} in $YAlO_3$; (b) polarized Raman spectra of $YAlO_3$ for the ***b***(*m*,*n*)***b*** geometry (*m*, *n* = ***a***, ***c***); (c) stimulated-emission cross-sections, σ_{SE}, for the $^4I_{11/2} \rightarrow {}^4I_{13/2}$ transition of Er^{3+} in $YAlO_3$ for light polarizations ***E*** || ***a***, ***b***, ***c***; (d) luminescence decay curves from the $^4I_{11/2}$ and $^4I_{13/2}$ Er^{3+} manifolds in $YAlO_3$.

A 10 at.% Er^{3+}-doped $YAlO_3$ crystal was grown by the Czochralski method [13]. $YAlO_3$ belongs to the orthorhombic class (sp. gr. *Pnma*) and it is optically biaxial. The optical indicatrix axes coincide with the crystallographic directions, and the principal light polarizations are ***E*** || ***a***, ***b***, ***c***. The stimulated-emission (SE) cross-sections, σ_{SE}, for the $^4I_{11/2} \rightarrow {}^4I_{13/2}$ transition of Er^{3+} in $YAlO_3$ were calculated by the Füchtbauer-Ladenburg equation based on the polarized luminescence spectra measured under N_2 atmosphere using the radiative lifetime of the $^4I_{11/2}$ state (τ_{rad} = 7.39 ms) and the luminescence branching ratio ($\beta_{JJ'}$ = 21.9%) obtained by the Judd-Ofelt analysis [14], see Fig. 1(c). The maximum σ_{SE} is 1.47×10^{-20} cm^2 at 2712 nm for ***E*** || ***b*** and in the long-wave spectral range where laser operation is expected, $\sigma_{SE} = 0.20\times10^{-20}$ cm^2 at 2919 nm for ***E*** || ***c***. The emission bandwidth of the latter peak (full width at half maximum, FWHM) is 10 nm. The luminescence decay from the $^4I_{13/2}$ and the $^4I_{11/2}$ levels was studied under resonant excitation by nanosecond laser pulses employing finely powdered samples to avoid radiation trapping. Luminescence lifetimes mean values of 6.68 and 1.08 ms were obtained respectively, see Fig. 1(d). At the high Er^{3+} doping level of 10 at.%, the ETU_1 rate is boosted which suppresses the bottleneck effect.

The laser set-up is shown in Fig. 2. The rectangular laser element (10 at.% Er:$YAlO_3$) was 5-mm thick along the light propagation direction (***a***-axis) with an aperture of 2(***b***)×2(***c***) mm^2. Both its faces were polished to laser quality and left uncoated. The crystal was mounted on a passively cooled Cu-holder using a silver paint. The hemispherical laser cavity was formed by a plane pump mirror (PM) coated for high transmission at the pump wavelength (T = 88% at 0.98 μm) and high reflectance at 2.6-3 μm, and a set of concave output couplers (OCs, RoC = -100 mm) with a transmission at the laser wavelength T_{OC} in the range of 0.33% - 4.0%. The crystal was placed close to the PM. The cavity length was ~99 mm. The pump source was a commercial YFL (Azur Light Systems, ALS-IR-122) emitting a near diffraction limited beam (M^2 = 1.02) at 975.8 nm (laser linewidth: 0.3 nm) addressing the $^4I_{15/2} \rightarrow {}^4I_{11/2}$ transition of Er^{3+}. After passing through an optical isolator, the collimated pump beam was focused into the crystal through the PM using an antireflection (AR) coated achromatic lens (f = 75 mm). The pump polarization was adjusted by an AR coated half-wave plate (λ/2) to correspond to ***E*** || ***b*** in the crystal. The measured single-pass pump absorption was weakly dependent on T_{OC} and incident pump power and amounted to 86.2% (considering the Fresnel losses). The residual pump after the OC was filtered out using a long-pass filter (F). The spectra of laser emission were measured using an optical spectrum analyzer (Yokogawa AQ6376) and a ZrF_4 fiber.

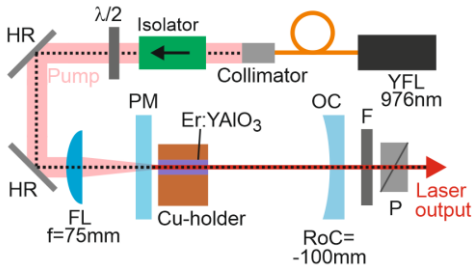

Fig. 2. Layout of the YFL pumped 3-μm Er:$YAlO_3$ laser: PM – pump mirror, OC – output coupler, FL – focusing lens; F – long-pass filter, P – polarizer, HR – highly-reflective mirror, RoC – radius of curvature.

The power transfer characteristics of the Er:$YAlO_3$ laser are shown in Fig. 3(a). A maximum output power of 1.36 W was achieved at 2919 nm with a slope efficiency η of 31.4% (versus the absorbed pump power), being close to the Stokes limit, $\eta_{StL} = \lambda_P/\lambda_L$ = 33.4%, and a low laser threshold of 33 mW when using an intermediate T_{OC} of 1.7 %. This corresponded to a maximum incident pump power of 5.3 W and an optical efficiency of 25.7%. Further power scaling was limited by the available pump power. The laser threshold decreased from 64 mW for T_{OC} = 4.0% down to 15 mW for T_{OC} = 0.33%. The input-output dependences were linear above the laser threshold without any signs of detrimental thermal effects or thermal fracture of the crystal. The laser was operating for hours without any degradation of output performance. The beam quality factors measured at the maximum pump power were $M^2_{x,y} < 1.5$. The slope efficiency of 2.8-μm Er lasers is determined by the ratio of ETU rates from the $^4I_{13/2}$ (ETU_1) and $^4I_{11/2}$ (ETU_2, $^4I_{11/2} + {}^4I_{11/2} \rightarrow {}^4F_{7/2} + {}^4I_{15/2}$) states which can be improved by optimizing the Er^{3+} doping level.

Typical spectra of laser emission measured well above the laser threshold are presented in Fig. 3(b). For all the studied OCs, the laser operated at 2919 nm and for the highest T_{OC} = 4%, an extra line at 2731 nm was observed. At high pump powers, $P_{abs} > 2.5$ W, the laser emission was linearly polarized (***E*** || ***c***) in line with the anisotropy of

the σ_{SE} spectra, see Fig. 1(c). More complex spectral behavior associated with a polarization switching was observed at low to intermediate absorbed pump powers. Figure 3(c) depicts representative laser spectra observed at different pump powers for the optimum T_{OC} of 1.7%. Near the threshold, the Er-laser operated at 2796 nm with a linear polarization $\boldsymbol{E} \parallel \boldsymbol{b}$. Upon increasing the pump level, two orthogonal eigen polarization states coexisted, $\boldsymbol{E} \parallel \boldsymbol{b}$ and $\boldsymbol{E} \parallel \boldsymbol{c}$, leading to generation of three laser lines, 2731, 2796 and 2919 nm. At even higher pump powers, polarization was $\boldsymbol{E} \parallel \boldsymbol{c}$ with emission solely at 2919 nm.

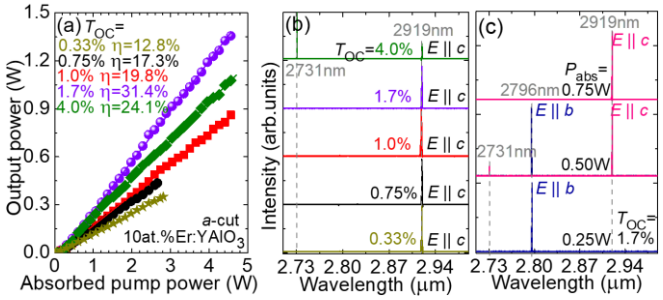

Fig. 3. 10 at.% Er:$YAlO_3$ laser: (a) input-output dependences, ***a***-cut crystal, η – slope efficiency; (b) spectra of laser emission measured well above the threshold; (c) polarization-resolved spectra as a function of absorbed pump power (P_{abs}) for T_{OC} = 1.7%.

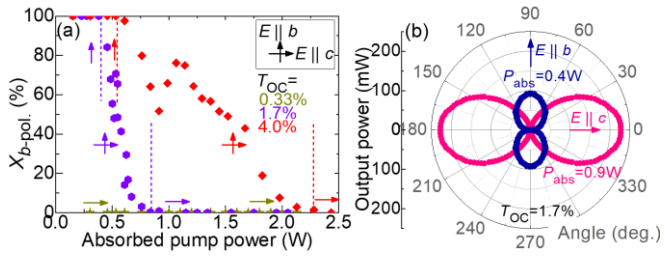

Fig. 4. Pump-induced polarization switching in the 3-μm Er:$YAlO_3$ laser: (a) Power fraction of emission with light polarization $\boldsymbol{E} \parallel \boldsymbol{b}$ ($X_{b\text{-pol.}}$) *vs.* absorbed pump power (P_{abs}) for different T_{OC}; (b) polarization state measurements for T_{OC} = 1.7% at different pump levels.

To better understand the polarization behavior of the Er:$YAlO_3$ laser, we measured the power fraction of laser emission with $\boldsymbol{E} \parallel \boldsymbol{b}$ polarization ($X_{b\text{-pol.}}$) versus the absorbed pump power for different T_{OC}, Fig. 4(a). For T_{OC} = 1.7% and 4%, the laser behavior was similar as discussed above. Upon increasing T_{OC}, the range of polarization switching shifted toward higher pump powers, going from 0.9 W for T_{OC}= 1.7% to 2.4W for T_{OC}= 4%. On the contrary, for very low T_{OC} of 0.33%, laser oscillation directly occurred at $\boldsymbol{E} \parallel \boldsymbol{c}$ even at the laser threshold and no switching was observed. Figure 4(b) shows the characterization of the polarization state of the Er laser emission for T_{OC} = 1.7% taken at P_{abs} = 0.4 W and 0.9 W, i.e., just below and above the range of polarization switching, respectively, showing that the laser emission was linearly polarized ($\boldsymbol{E} \parallel \boldsymbol{b}$ and $\boldsymbol{E} \parallel \boldsymbol{c}$, respectively) corresponding to a polarization degree P > 99.9%.

Polarization switching in solid-state lasers based on birefringent crystals implying no polarization-selective elements is known. Two major mechanisms were suggested to explain such behavior: (i) polarization anisotropy of thermal lensing affecting the diffraction losses in the laser cavity, its stability conditions or mode-matching efficiency, and (ii) relative closeness of gain profiles for eigen polarization states causing mode competition [17, 18].

The operation of 3-μm Er lasers is similar to a quasi-three-level scheme due to reabsorption from the metastable terminal laser level associated with a resonant excited-state absorption (ESA), $^4I_{13/2} \rightarrow {}^4I_{11/2}$. One can access the ESA spectra by calculating them using the reciprocity principle based on the crystal-field splitting of the two multiplets involved in the transition. Figure 5 shows the low temperature (12 K) polarized absorption spectra of Er^{3+} in $YAlO_3$ for the $^4I_{15/2} \rightarrow {}^4I_{11/2}$ and $^4I_{15/2} \rightarrow {}^4I_{13/2}$ transitions. Er^{3+} ions in $YAlO_3$ replace for Y^{3+} cations in C_s symmetry sites with VIII-fold oxygen coordination. In this crystal field, the $^{2S+1}L_J$ multiplets are split into J + 1/2 sub-levels. By resolving all electronic transitions of the Er^{3+} ion, the experimental Stark splitting of the $^4I_{11/2}$ and $^4I_{13/2}$ multiplets was determined as shown in Fig. 5. The zero-phonon line (ZPL) transition energy E_{ZPL} is 3690 cm^{-1} matching the most intense peak in the SE spectra (2710 nm), and the partition functions of the upper (Z_u) and lower (Z_l) multiplets at room temperature are 4.141 and 4.640, respectively, so that Z_l/Z_u = 0.892.

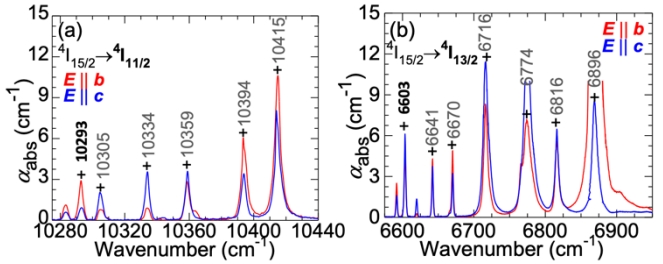

Fig. 5. (a,b) Low temperature (12 K) absorption spectra of Er:$YAlO_3$: (a) the $^4I_{15/2} \rightarrow {}^4I_{11/2}$ transition; (b) the $^4I_{15/2} \rightarrow {}^4I_{13/2}$ transition, $\boldsymbol{E} \parallel \boldsymbol{b}$ and $\boldsymbol{E} \parallel \boldsymbol{c}$ light polarizations, "+" indicate electronic transitions.

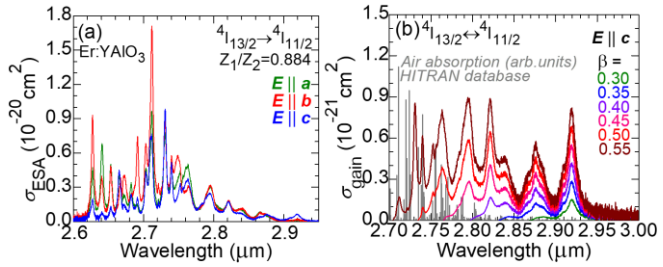

Fig. 6. Excited-state absorption of Er^{3+} in $YAlO_3$: (a) ESA cross-sections, σ_{ESA}, for the $^4I_{13/2} \rightarrow {}^4I_{11/2}$ transition for light polarizations $\boldsymbol{E} \parallel \boldsymbol{a}, \boldsymbol{b}, \boldsymbol{c}$; (b) gain cross-sections, σ_{gain}, around 3 μm for light polarization $\boldsymbol{E} \parallel \boldsymbol{c}$, β - inversion ratio. *Grey lines* – water vapor absorption in air.

The ESA cross-sections, σ_{ESA}, for the principal light polarizations $\boldsymbol{E} \parallel \boldsymbol{a}, \boldsymbol{b}, \boldsymbol{c}$ are given in Fig. 6(a). The maximum σ_{ESA} value amounts to 1.71×10^{-20} cm^2 at 2712 nm (ZPL, for $\boldsymbol{E} \parallel \boldsymbol{b}$) and at the dominant laser wavelength of 2919 nm, σ_{ESA} amounts to 0.06×10^{-20} cm^2 (for $\boldsymbol{E} \parallel \boldsymbol{c}$). The gain cross-sections can be defined as $\sigma_{gain} = \beta\sigma_{SE} - (1 - \beta\sigma_{ESA})$, where $\beta = N_3/(N_2 + N_3)$ is the inversion ratio, $N_1 + N_2 + N_3 \approx N_{Er}$ and N_i (i = 1, 2, 3) are the populations of the $^4I_{15/2}$, $^4I_{13/2}$ and $^4I_{11/2}$ manifolds, respectively. Figure 6(b) gives the gain profiles of Er^{3+} in

$YAlO_3$ in the 2.7 to 3 μm range indicating that depending on the inversion level, multiple laser lines between 2.73 and 2.92 μm can be supported. However, lasing on some of them is suppressed by intense water vapor absorption lines in atmospheric air, Fig. 6(b).

To explain the observed polarization behavior of the Er:$YAlO_3$ laser, we consider the polarization anisotropy of the gain properties of the Er^{3+} ion. For an ***a***-cut crystal, the eigen polarizations are $\boldsymbol{E} \parallel \boldsymbol{b}$ and $\boldsymbol{E} \parallel \boldsymbol{c}$. The operation of this laser can be subjected to variation in the inversion ratio β when changing the pump level. Indeed, owing to the longer lifetime of the terminal laser level ($^4I_{13/2}$) compared to that of the upper laser state ($^4I_{11/2}$), on increasing the pump power, the ions will accumulate in the lower laser level, resulting in a reduction of β. In Fig. 7(a-c), we plot the gain profiles for $\boldsymbol{E} \parallel \boldsymbol{b}$ and $\boldsymbol{E} \parallel \boldsymbol{c}$ and three different inversion ratios around 0.5, a value commonly achieved in Er lasers operating on the $^4I_{11/2} \rightarrow {}^4I_{13/2}$ transition. For higher β of 0.55, the dominant peak in the gain spectra is at 2796 nm for $\boldsymbol{E} \parallel \boldsymbol{b}$. For an intermediate β of 0.50, two peaks at 2796 nm ($\boldsymbol{E} \parallel \boldsymbol{b}$) and 2919 nm ($\boldsymbol{E} \parallel \boldsymbol{c}$) correspond to almost equal gain which is a prerequisite for colasing on both polarization states. For lower β of 0.45, the latter peak at 2919 nm for $\boldsymbol{E} \parallel \boldsymbol{c}$ becomes dominant. In addition, there is no effect of the air/water absorption as seen in Fig. 6b at these two wavelengths. This analysis well explains the observed spectral and polarization behavior of the Er:$YAlO_3$ laser. It can be further illustrated by plotting σ_{gain} values at two respective wavelengths for two orthogonal polarizations as a function of β as shown in Fig. 7(d). The laser will always choose the trajectory with the highest gain, so that the crossing of the two higher-lying $\sigma_{gain}(\beta)$ curves will correspond to the point of polarization-switching and dual-wavelength operation. Due to the moderate anisotropy of emission properties of Er^{3+} and possible polarization anisotropy of thermal lensing, the switching occurs over a certain range of pump powers, but not at a single point.

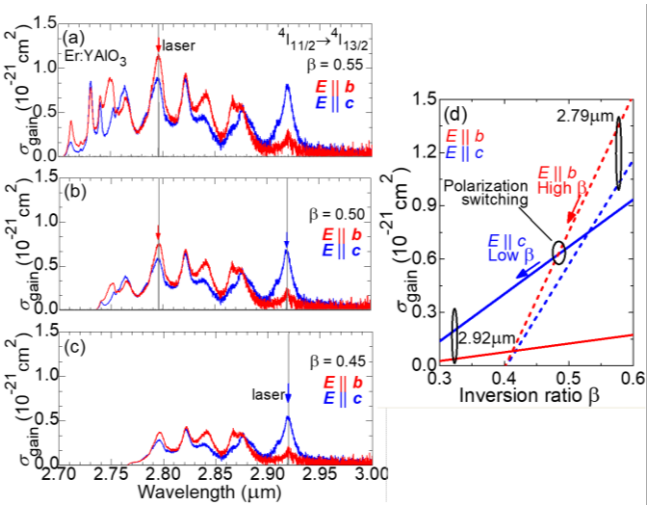

Fig. 7. Explanation of polarization switching in the 3-μm Er:$YAlO_3$ laser (***a***-cut): (a-c) gain cross-section, σ_{gain}, spectra for the $^4I_{11/2} \rightarrow {}^4I_{13/2}$ transition for the two orthogonal light polarizations, $\boldsymbol{E} \parallel \boldsymbol{b}$ and $\boldsymbol{E} \parallel \boldsymbol{c}$ and different inversion ratios β: (a) $\beta = 0.55$, (b) $\beta = 0.50$, and (c) $\beta = 0.45$; (d) dependence of σ_{gain} at 2.79 μm (*dashed lines*) and 2.92 μm (*solid lines*) on the inversion ratio for $\boldsymbol{E} \parallel \boldsymbol{b}$ (*in red*) and $\boldsymbol{E} \parallel \boldsymbol{c}$ (*in blue*).

To conclude, the observed polarization anisotropy of stimulated -emission and gain cross-section spectra of Er^{3+} in $YAlO_3$ enabled us to explain several effects in 3 μm Er:$YAlO_3$ lasers: (i) linearly polarized emission at 2.92 μm from such lasers at high power levels, (ii) evolution of laser spectra with pump power (by accounting for the resonant excited-state absorption from the terminal laser level) and (iii) pump-induced switching between two eigen polarization states. We also show a proof-of-concept of using commercial high-brightness Yb-fiber lasers at 976 nm for efficient pumping of Er:$YAlO_3$ crystals leading to extremely low laser thresholds and high overall optical efficiency. Our YFL pumped Er:$YAlO_3$ laser generated Watt-level output power at 2919 nm with a slope efficiency of 31.4%, a laser threshold as low as 33 mW and a linear polarization.

Funding. French Agence Nationale de la Recherche (ANR, project SPLENDID2, ANR-19-CE08-0028); European project NOVAMAT; Région Normandie (Chaire d'excellence "RELANCE"); National Natural Science Foundation of China (61975208); Sino-German Scientist Cooperation and Exchanges Mobility Program (M-0040).

Disclosures. The authors declare no conflicts of interest.

Data availability. Data underlying the results presented in this paper are not publicly available at this time but may be obtained from the authors upon reasonable request.

References

1. T. H. Allik, S. Chandra, D. M. Rines, P. G. Schunemann, J. A. Hutchinson, and R. Utano, Opt. Lett. **22**, 597 (1997).
2. T. S. Saini, N. P. T. Hoa, K. Nagasaka, X. Luo, T. H. Tuan, T. Suzuki, and Y. Ohishi, Appl. Opt. **57**, 1689 (2018).
3. E. Li, H. Uehara, W. Yao, S. Tokita, F. Potemkin, and R. Yasuhara, Opt. Express **29**, 44118 (2021).
4. R. I. Woodward, M. R. Majewski, G. Bharathan, D. D. Hudson, A. Fuerbach, and S. D. Jackson, "Opt. Lett. **43**, 1471 (2018).
5. C. Bader and I. Krejci, Am. Journal of Dentistry **19**, 178 (2006).
6. J. Ma, Z. Qin, G. Xie, L. Qian, and D. Tang, Appl. Phys. Rev. **6**, 021317 (2019).
7. R. Švejkar, J. Šulc, and H. Jelínková, Progr. Quantum Electron. **74**, 100276 (2020).
8. M. Pollnau, Th. Graf, J. E. Balmer, W. Lüthy, and H. P. Weber, Phys. Rev. A. **49**, 3990 (1994).
9. S. Tokita, M. Murakami, S. Shimizu, M. Hashida, and S. Sakabe, Opt. Lett. **34**, 3062 (2009).
10. W. Yao, H. Uehara, H. Kawase, H. Chen, and R. Yasuhara, Opt. Express **28**, 19000 (2020).
11. L. Guillemot, P. Loiko, A. Braud, J.-L. Doualan, A. Hideur, M. Koselja, R. Moncorge, and P. Camy, Opt. Lett. **44**, 5077 (2019).
12. W. Yao, H. Uehara, E. Li, and R. Yasuhara, Opt. Laser Technol. **152**, 108073 (2022).
13. C. Quan, D. Sun, H. Zhang, J. Luo, L. Hu, Z. Han, Y. Qiao, K. Dong, Y. Chen, and M. Cheng, J. Lumin. **251**, 119122 (2022).
14. D. K. Sardar, S. Chandrasekharan, K. L. Nash, and J. B. Gruber, Journal of App. Phys. **104**, 023102 (2008).
15. V. A. Antonov, P. A. Arsenev, K. E. Bienert, and A. V. Potemkin, Phys. Stat. Sol. (A) **19**, 289 (1973).
16. W. Yao, E. Li, H. Uehara, and R. Yasuhara, Opt. Express **29**(16), 24606-24613 (2021).
17. P.A. Loiko, X. Mateos, N.V. Kuleshov, A.A. Pavlyuk, K.V. Yumashev, V. Petrov, U. Griebner, M. Aguiló, and F. Díaz, IEEE J. Quantum Electron. **50**, 669 (2014).
18. F. Druon, M. Olivier, A. Jaffrès, P. Loiseau, N. Aubry, J. DidierJean, F. Balembois, B. Viana, and P. Georges, Opt. Lett. **38**, 4138 (2013).

Full references

1. T. H. Allik, S. Chandra, D. M. Rines, P. G. Schunemann, J. A. Hutchinson, and R. Utano, "Tunable 7-12 µm optical parametric oscillator using a Cr,Er:YSSG laser to pump CdSe and $ZnGeP_2$ crystals," Opt. Lett. **22**(9), 597-599 (1997).
2. T. S. Saini, N. P. T. Hoa, K. Nagasaka, X. Luo, T. H. Tuan, T. Suzuki, and Y. Ohishi, "Coherent midinfrared supercontinuum generation using a rib waveguide pumped with 200 fs laser pulses at 2.8 µm," Appl. Opt. **57**(7), 1689-1693 (2018).
3. E. Li, H. Uehara, W. Yao, S. Tokita, F. Potemkin, and R. Yasuhara, "High-efficiency, continuous-wave Fe:ZnSe mid-IR laser end pumped by an Er:YAP laser," Opt. Express **29(**26), 44118-44128 (2021).
4. R. I. Woodward, M. R. Majewski, G. Bharathan, D. D. Hudson, A. Fuerbach, and S. D. Jackson, "Watt-level dysprosium fiber laser at 3.15 µm with 73 % slope efficiency," Opt. Lett. **43**(7), 1471-1474 (2018).
5. C. Bader and I. Krejci, "Indications and limitations of Er:YAG laser applications in dentistry," Am. Journal of Dentistry **19**(3)**,** 178 (2006).
6. J. Ma, Z. Qin, G. Xie, L. Qian, and D. Tang, "Review of mid-infrared mode-locked laser sources in the 2.0 µm–3.5 µm spectral region," Appl. Phys. Rev. **6**(2), 021317 (2019).
7. R. Švejkar, J. Šulc, and H. Jelínková, "Er-doped crystalline active media for ~3 µm diode-pumped lasers," Progr. Quantum Electron. **74**, 100276 (2020).
8. M. Pollnau, Th. Graf, J. E. Balmer, W. Lüthy, and H. P. Weber, "Explanation of the cw operation of the Er^{3+} 3-µm crystal laser," Phys. Rev. A. **49**(5), 3990-3996 (1994).
9. S. Tokita, M. Murakami, S. Shimizu, M. Hashida, and S. Sakabe, "Liquid-cooled 24 W mid-infrared Er:ZBLAN fiber laser," Opt. Lett. **34**(20), 3062-3064 (2009).
10. W. Yao, H. Uehara, H. Kawase, H. Chen, and R. Yasuhara, "Highly efficiency Er:YAP laser with 6.9 W of output power at 2920 nm," Opt. Express **28**(13), 19000-19007 (2020).
11. L. Guillemot, P. Loiko, A. Braud, J.-L. Doualan, A. Hideur, M. Koselja, R. Moncorge, and P. Camy, "Continuous-wave Tm:$YAlO_3$ laser at ~2.3 µm," Opt. Lett. **44**(20), 5077-5080 (2019).
12. W. Yao, H. Uehara, E. Li, and R. Yasuhara, "Power-scalable two-wavelength pumped Er:YAP laser at 2.9 µm," Opt. Laser Technol. **152**, 108073 (2022).
13. C. Quan, D. Sun, H. Zhang, J. Luo, L. Hu, Z. Han, Y. Qiao, K. Dong, Y. Chen, and M. Cheng, "Growth, spectroscopy and high-power laser operation of Er:YAP crystal with different Er^{3+} concentrations," J. Lumin. **251**, 119122 (2022).
14. D. K. Sardar, S. Chandrasekharan, K. L. Nash, and J. B. Gruber, "Optical intensity analyses of Er^{3+}:$YAlO_3$," Journal of App. Phys. **104(**2), 023102 (2008).
15. V. A. Antonov, P. A. Arsenev, K. E. Bienert, and A. V. Potemkin, "Spectral properties of rare-earth ions in $YAlO_3$ crystals," Phys. Stat. Sol. (A) **19**, 289-299 (1973).
16. W. Yao, E. Li, H. Uehara, and R. Yasuhara, "Efficient diode-pumped Er:YAP master-oscillator power-amplifier system for laser power improvement at 2920 nm," Opt. Express **29**(16), 24606-24613 (2021).
17. P.A. Loiko, X. Mateos, N.V. Kuleshov, A.A. Pavlyuk, K.V. Yumashev, V. Petrov, U. Griebner, M. Aguiló, and F. Díaz, "Thermal-lens-driven effects in Ng-cut Yb- and Tm-doped monoclinic $KLu(WO_4)_2$ crystals," IEEE J. Quantum Electron. **50**(8), 669-676 (2014).
18. F. Druon, M. Olivier, A. Jaffrès, P. Loiseau, N. Aubry, J. DidierJean, F. Balembois, B. Viana, and P. Georges, "Magic mode switching in Yb:$CaGdAlO_4$ laser under high pump power," Opt. Lett. **38**(20), 4138-4141 (2013).